Selenium Thin-Film Solar Cells with Cadmium Sulfide as a Heterojunction Partner

Nielsen, Rasmus; Youngman, Tomas H.; Crovetto, Andrea; Hansen, Ole; Chorkendorff, Ib; Vesborg, Peter C.K.

Published in:
ACS Applied Energy Materials

Link to article, DOI:
10.1021/acsaem.1c01700

Publication date:
2021

Document Version
Peer reviewed version

Selenium thin-film solar cells with cadmium sulfide as a heterojunction partner

Rasmus Nielsen,*,† Tomas H. Youngman,† Andrea Crovetto,‡ Ole Hansen,¶ Ib Chorkendorff,† and Peter C. K. Vesborg*,†

†*SurfCat, DTU Physics, Technical University of Denmark, DK-2800 Kgs. Lyngby, Denmark*

‡*Department of Structure and Dynamics of Energy Materials, Helmholtz-Zentrum Berlin für Materialien und Energie GmbH, Berlin, Germany.*

¶*DTU Nanolab, National Center for Nano Fabrication and Characterization, Technical University of Denmark, DK-2800, Kgs. Lyngby, Denmark.*

E-mail: raniel@dtu.dk; Peter.Vesborg@fysik.dtu.dk

Abstract

Elemental selenium (Se) is experiencing a renaissance as a p-type direct wide bandgap (1.95 eV) photoabsorber, appropriate for integration with lower bandgap materials in tandem photovoltaic devices. However, single-junction selenium devices are typically in the superstrate configuration with the charge-separating p-n junction located very close to the substrate. For tandem devices, the p-n junction should ideally lie near the surface of the cell to maximize photocarrier collection, implying that the n-type heterojunction partner should be deposited on top of Se. Since Se is a soft, low melting point material, a low-damage deposition technique should then be identified for the partner material. Here, we investigate the suitability of CdS grown by chemical bath deposition as an n-type partner for Se cells. We demonstrate the first

functioning CdS/Se solar cell in the standard superstrate configuration. Although it may be possible to realize a substrate configuration, we find that the bandgap and electron affinity of CdS are not optimal for efficient carrier absorption and transport in selenium devices, suggesting that CdS is a poor partner for selenium.

Keywords

Selenium; cadmium sulfide; heterojunction; energy band diagram; chemical bath deposition; wide bandgap absorber; tandem solar cell.

Introduction

Silicon-based photovoltaic modules have exhibited the most rapid cost decline among all energy technologies,[1] shifting the overall cost of photovoltaic systems from being dominated by module costs to being dominated by balance-of-system costs.[2] As a consequence, research must focus on the area-related balance-of-system costs in order to further reduce the cost of photovoltaics. High-efficiency concepts require fewer installed modules to reach the same system power capacity, and may therefore be more economically feasible as opposed to low-cost–low-efficiency approaches.[3] However, the certified record power conversion efficiency (PCE) of single-junction silicon solar cells has only increased from 25.0% to 26.7% in the past 20 years,[4] asymptotically approaching the Shockley-Queisser (SQ) efficiency limit of single-junction devices.[5]

Tandem solar cells are a promising technology for surpassing the SQ limit, where two photoabsorbers of different bandgaps are integrated into a single device to reduce thermalization losses. The ideal combination of bandgaps (0.9 eV and 1.6 eV) allows for reaching a PCE = 45% without even having to concentrate sunlight,[3] but devices featuring silicon or Cu(In,Ga)Se_2 (CIGS) with $E_g \approx 1.1$ eV as the lower bandgap photoabsorber would likely be of higher commercial relevance. The ideal photoabsorbing material to match silicon or CIGS

in a tandem device should have a wide bandgap of $E_g \approx 1.75$ eV, but only few candidates in this range have shown high performance,[6] including metal-halide perovskites where long term degradation issues must be addressed[7–9] and III-V semiconductors that are cost-ineffective with respect to large-scale applications.[10,11]

Polycrystalline selenium (poly-Se), is another potential candidate with a reported direct bandgap of $E_g = 1.95$ eV in its trigonal phase. In addition to its suitable bandgap, poly-Se is an inexpensive single-element semiconductor, it has a high absorption coefficient ($\alpha > 10^5$ cm^{-1}) in the visible region, and its low melting point ~ 220°C makes it process compatible for low-cost monolithic integration with most bottom cell material candidates. However, recent work on bifacial selenium solar cells shows how the PCE is reduced by a factor of ~ 2 when illuminating through the p-type contact.[12] This reduction is believed to be a consequence of low carrier lifetimes and carrier diffusion lengths in poly-Se thin films. As a result, charge carriers generated outside the depletion region would have a low probability of being collected before recombining. The standard process flow for fabricating selenium solar cells implies that the p-type contact would be facing the Sun, if transferred directly onto a bottom cell. It is therefore critical to invert the structure, going from a superstrate configuration where the device is illuminated through the first deposited layers, to a substrate configuration where the device is illuminated through the final deposited layers.

The n-type contact materials in state-of-the-art selenium solar cells are typically deposited using magnetron sputtering. However, this deposition technique entails a bombardment of the sample surface with a variety of high-energy species,[13] which is detrimental for the interface in the carrier separating p-n junction, which is known to be highly sensitive to defects. Therefore, the introduction of a ≥ 10 nm protective buffer layer using a more gentle deposition technique is preferred to sputter depositing an n-type contact directly onto the poly-Se photoabsorber. The commonly used buffer layer cadmium sulfide (CdS) may be deposited using a chemical bath below 100°C, and has played a key role in the development of CIGS and the current record $Cu_2ZnSn(S,Se)_4$ (CZTS) solar cells.[14,15]

The general selection criteria for an appropriate n-type contact material include: i) A well aligned conduction band minimum at the heterointerface to facilitate efficient electron transfer. ii) A large bandgap to efficiently block holes and limit parasitic absorption losses. iii) Stability during processing and resistance against heat, UV light, moisture, and oxygen exposure. iv) Low processing and material cost. In the context of CdTe-based thin-film solar cells, CdS has already proven its stability after > 25 years of operation in the field as well as its commercial viability in terms of processing and material cost.[16]

In this work, the suitability of CdS as an n-type heterojunction partner to poly-Se is investigated by fabricating single-junction solar cells employing the champion structure FTO/n-type buffer/Te/Se/MoO_x/Au as reported by Todorov et al.[17] This device architecture is still in the superstrate configuration, but it serves as a starting point to examine the candidacy of CdS prior to inverting the structure. The process flow is based on an optimized in-house recipe resulting in devices with a PCE = 5.2%, where RF-sputtered ZnMgO has been used as the n-type contact material.[12] The energy band positions of CdS and poly-Se are investigated using photoelectron spectroscopy combined with optical transmission measurements, and the overall device performance is finally assessed of the first reported CdS/Se solar cell.

Experimental details

FTO-coated soda lime glass (SLG) substrates from Sigma Aldrich are cut to the dimensions 14 mm x 16 mm, and sequentially cleaned in an ultrasonic bath with Milli-Q water, acetone and isopropanol. The substrates are dried using a nitrogen-gun, and subsequently clamped onto teflon tweezers. The tweezers are dipped into a chemical bath contained in a 300 ml chemical reactor. The bath is composed of the following initial solutions: 215 ml Milli-Q water, 20 ml cadmium sulfate (0.06 M $CdSO_4$), 20 ml thiourea (1 M $SC(NH_2)_2$), and 25 ml ammonium hydroxide (15.3 M NH_3). The reactor is submerged into a pre-heated water bath at 60°C, and magnetic stirrers are employed at 120 RPM in both the reactor and the

water bath. After 8 minutes ∼50 nm CdS has been deposited, and the samples are brought out of the bath and ultrasonically cleaned in Milli-Q for 5 minutes. The film formed on the unintended side of the substrate is removed using a cotton swap dipped in HCl.[18]

The CdS/FTO/SLG samples are brought into a custom-built thermal evaporator at a base pressure of 1×10^{-6} Torr. Here, ≈ 1 nm Te and ≈ 300 nm Se are thermally evaporated onto the samples using deposition rates of ≈ 0.25 Å s^{-1} and ≈ 4 Å s^{-1}, respectively. The samples are then annealed in air at $\approx 190°C$ for 4 minutes in a home-built aluminium mini oven. After crystallizing the selenium photoabsorber, ∼15 nm MoO_x is reactively DC-sputtered from a metallic Mo-target. The samples are re-annealed using the same conditions as before to cure sputter-damage and further oxidize the MoO_x hole-transport layer. Finally, Au-contacts are deposited using DC-sputtering, and once again the samples are re-annealed to cure sputter-damage.

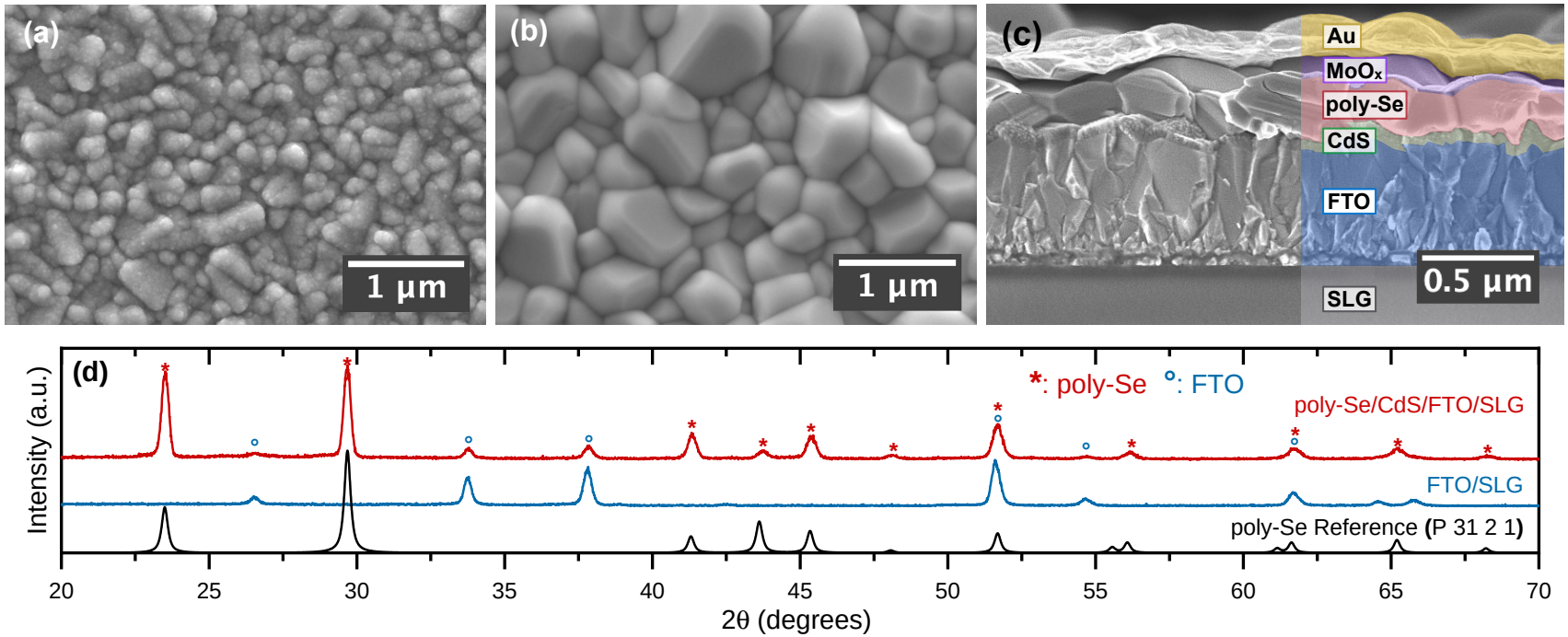

Figure 1: (a) Top-view SEM image of CdS on FTO. (b) Top-view of poly-Se grown on CdS/FTO. (c) Cross-section of the final device. The delamination of the Au contact is a result of the device being mechanically cracked in order to perform cross-sectional SEM-imaging. (d) The corresponding GIXRD-patterns of poly-Se and the FTO-coated glass substrate compared to a simulated XRD-pattern of randomly oriented trigonal selenium (collection code 40018 in the Inorganic Crystal Structure Database, ICSD).

Results and discussion

Top-view scanning electron microscopy (SEM) images of the chemical bath deposited CdS-film and the poly-Se grains are shown in Fig. 1a and b, respectively. The bath conditions have been optimized to obtain a full coverage of the CdS-film on the inherently rough surface of the FTO-substrate. The morphology of the Se layer grown on CdS is similar to the case of Se grown on the standard n-type partner TiO_2,[19] with crystal grains extending from top to bottom and no apparent pinholes (Fig. 1c).

Grazing incidence X-ray diffraction (GIXRD) patterns of the FTO-coated substrate and poly-Se synthesized on CdS are shown in Fig. 1d along with a simulated diffraction pattern of randomly oriented trigonal selenium. All of the peaks in the poly-Se diffraction pattern are either expected for trigonal selenium or accounted for by the FTO-coated substrate. The relative intensity of the (100)-peak at $\sim 24^\circ$ to the (101)-peak at $\sim 30^\circ$ implies that the distribution of lattice planes parallel to the surface of the photoabsorber is somewhat different than a randomly oriented polycrystalline film. As the trigonal phase of selenium is highly anisotropic, several optoelectronic properties may influence device performance as the orientation of the crystal grains change with respect to that of the substrate, e.g. the charge extraction as described by Hadar et al.[20] The reason for this preferential growth direction is not clear and has not been observed in our previous in-house studies, where trigonal selenium has been synthesized on a number of different contact materials using similar crystallization conditions.

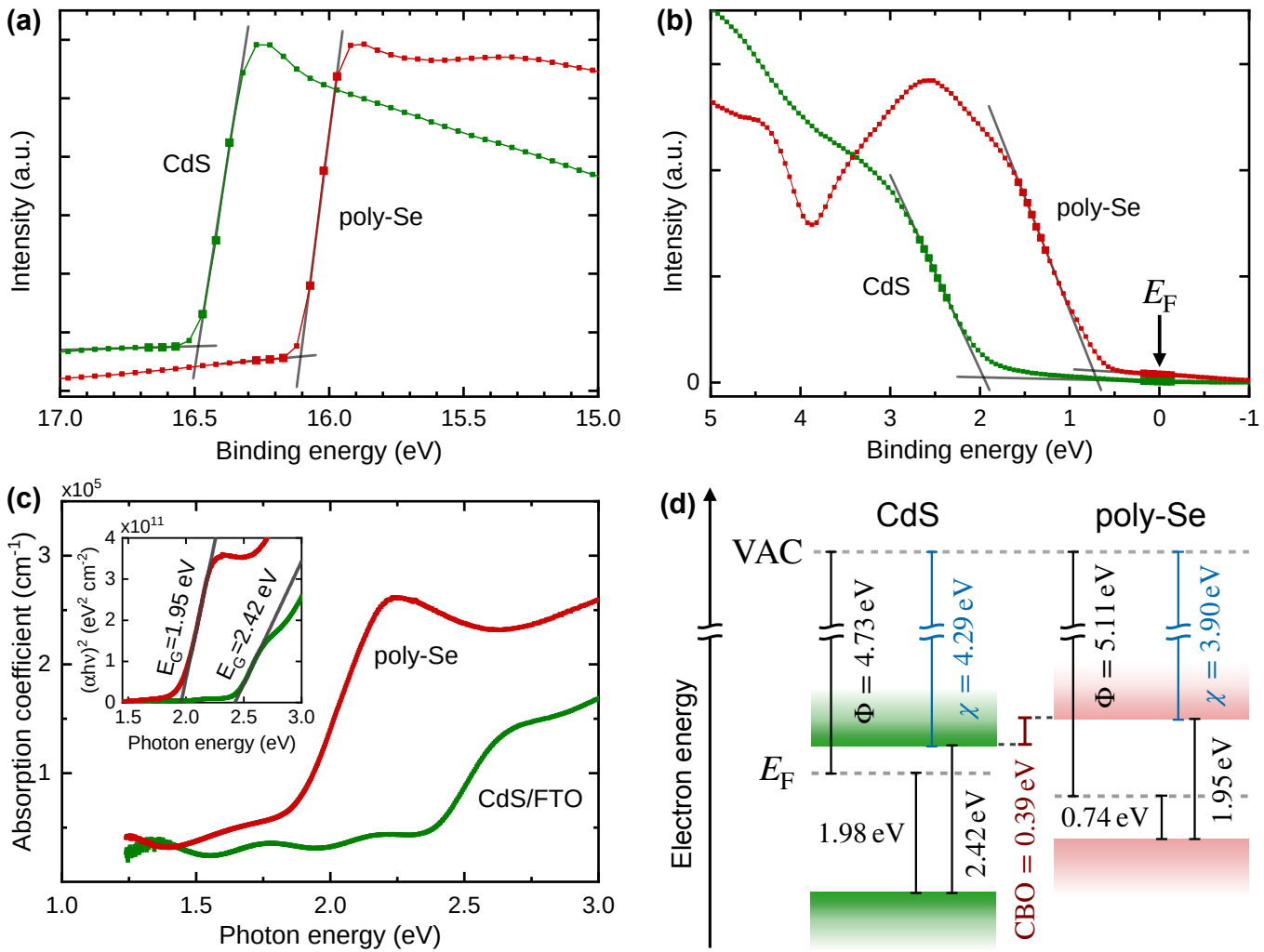

Figure 2: UPS analysis ion-etch cleaned CdS and poly-Se at (a) the secondary electron cut-off, and (b) the valence band maxima relative to the Fermi-level. A small bias of -5 V has been applied to the sample surface as to deconvolute the work function of the surface from that of the energy analyzer. (c) Absorption coefficients and Tauc-plots derived from UV-Vis transmission measurements. The optical bandgaps of CdS and poly-Se are linearly extrapolated from the onset of the Tauc-plots. (d) The resulting energy band diagrams with reference to a common vacuum level.

The energy band alignment of CdS and poly-Se is studied using ultraviolet photoelectron spectroscopy (UPS) combined with ultraviolet-visible (UV-Vis) spectroscopy. As the two samples have been air-exposed, the surface is cleaned using a mild Ar^+ ion beam etch (300 eV, 2 min) in a 2 mm x 2 mm raster to remove surface contaminants. To deconvolute the true work function of the surfaces from that of the energy analyzer, a small bias of -5 V is applied to the sample surfaces, shifting the entire UPS-spectra to higher kinetic energies. The secondary electron cut-offs and valence band offsets relative to the Fermi-level are shown on a binding energy scale in Fig. 2a and b, respectively. The electronic work functions of the sample surfaces are acquired by subtracting the low energy cut-offs from the narrow He-I line at 21.22 eV. The absorption coefficients are calculated from the UV-Vis transmission measurements using Lambert-Beers law and plotted in Fig. 2c along with the derived Tauc-plots. The optical bandgaps are determined by extrapolating the onsets of the linear regimes in the Tauc-plots, and the resulting energy band diagrams of CdS and poly-Se are plotted in Fig. 2d. The band positions of CdS match previously reported values.[21]

The energy band positions in Fig. 2d have been plotted with reference to a common vacuum level, as the electron affinity is considered to be a material constant. On the contrary, the work function and the position of the Fermi-level with respect to that of the energy bands are determined by the charge carrier density, which is dependent on processing conditions that may vary the density of impurities and defects. In a simple Anderson model,[22] the difference in electron affinities determines the discontinuity in the conduction band at the junction, whereas the total drop in the conduction band energy when crossing the depletion region is obtained by aligning the Fermi-levels of the two semiconductors. The total conduction band energy drop includes any offsets at the junction caused by interfacial mechanisms such as Fermi-level pinning and chemical interdiffusion, which is not considered in this work.[23,24] We report a conduction band offset (CBO) of 390 meV, a band bending of 380 meV, and a total conduction band energy drop of 770 meV, which is expected to significantly reduce the open-circuit voltage of the final device.

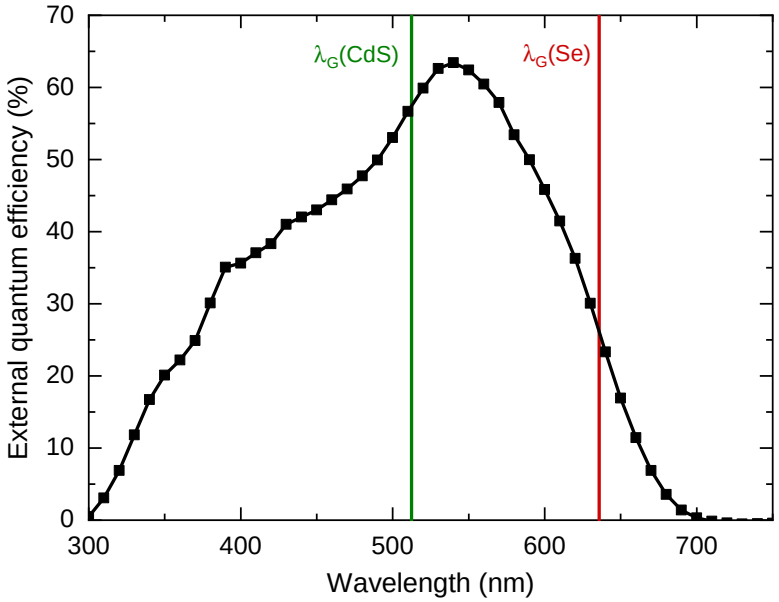

Figure 3: External quantum efficiency measurement of the final device. The optical bandgaps of CdS and poly-Se extrapolated from Tauc-plots have been inserted. The proximity of the bandgap of CdS to that of poly-Se is clearly expected to cause a severe loss of current due to loss of photons below 500 nm in wavelength.

The external quantum efficiency (EQE) measurement of the final device is shown in Fig. 3. The FTO-substrates used in this study have $\approx 80\%$ transmittance in the visible region, and should thus only account for a small portion of the EQE-loss at higher wavelengths. The optical bandgaps of CdS and poly-Se have been inserted to exhibit the parasitic absorption losses in CdS. As the bandgap of CdS is relatively low when compared to that of poly-Se, and the absorption coefficient is relatively high, the blue light is lost in the CdS and the short-circuit current density integrated over the EQE spectrum is $J_{\mathrm{SC}} = 7.83$ mA/cm^2.

The overall performance of the CdS/Se solar cell has been assessed from the current-voltage (J-V) characteristics shown in Fig. 4. To eliminate any spectral mismatch from the solar simulator as well as internal reflection from outside the active area of the device,[17] the short-circuit current density has been normalized to that obtained from the EQE-measurement. Finally, we report a power conversion efficiency PCE $\approx 1.14\%$ with an open-circuit voltage of $V_{\mathrm{OC}} = 472$ mV, and a fill factor of FF $= 30.8\%$.

Once the conduction band offset had been measured, it was no surprise that the device

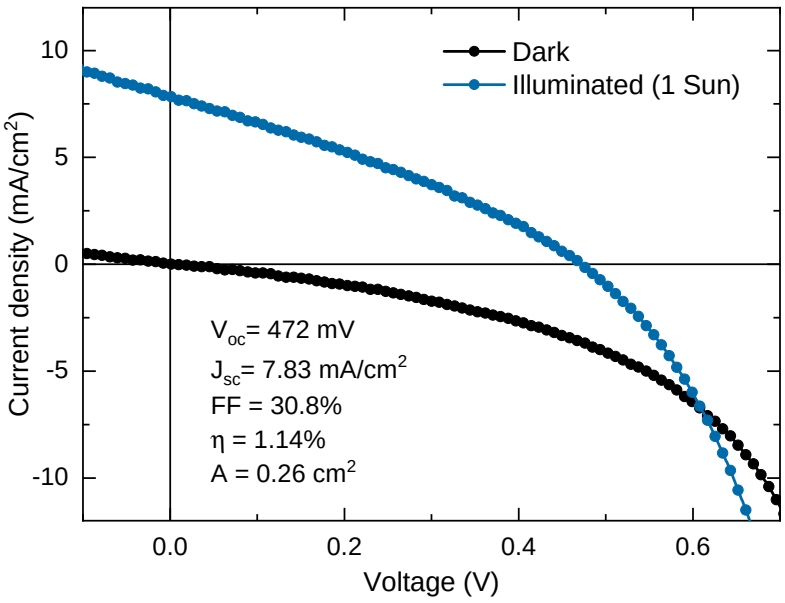

Figure 4: Measured current density–voltage (J-V) curve of the final CdS/Se solar cell under dark (*black*) and illuminated (*blue*) conditions. The short-circuit current density J_{SC} has been calibrated with the integrated current density from the EQE-measurement.

performance was poor. To maximize the efficiency of a heterojunction solar cell, the conduction band minimum (CBM) of the p-type photoabsorber should lie about 0-0.4 eV below the CBM of its n-type heterojunction partner at the interface.[14,25] Similar to the champion CZTS solar cell employing a CdS protection layer deposited using a chemical bath,[15] the conduction band offset at the CdS/CZTS-interface is believed to play a major role in limiting the efficiency of the device.[26] The position of the Fermi-level in CdS may be shifted by tuning the processing parameters to change the density of impurities and defects, but as the electron affinity is a material constant and should be better aligned for efficient transport of electrons, CdS does not hold great promise as a partner for poly-Se.

Initial attempts of inverting the device structure has been carried out, where CdS was successfully deposited on poly-Se (Fig. S.12 in the Supplementary Material). The MoO_x hole-transport layer had to be excluded from the inverted design, as the film immediately dissolved in the chemical bath. However, the inverted devices did not show any photoactivity, and further studies using CdS are discouraged by the aforementioned fundamental mismatch

between CdS and poly-Se.

CdO and CdSe have previously been investigated as n-type contact materials in Se-based solar cells with more promising efficiencies than CdS.[27,28] While reducing the thickness of CdS can minimize parasitic absorption losses at wavelengths $\lambda < 520$ nm, an alternative approach is to oxygenate the buffer layer. Oxygenated CdS (CdS:O) has been widely studied in the optimization of CdTe thin-film solar cells and is known to increase the optical bandgap and upshift the conduction band minimum compared to that of pure CdS,[29–31] making it an altogether more suitable heterojunction partner for poly-Se. However, realizing the necessary control of the elemental composition and the mixture of CdS, $CdSO_4$ and $CdSO_3$ phases rather than a single CdS_xO_{1-x} phase is usually accomplished using reactive sputtering[29,32] or by annealing the chemical bath deposited films under a high partial pressure of oxygen at temperatures significantly above the melting temperature of elemental selenium.[33] Recent work published by Liu et al. shows a successful inversion of the device polarity of a selenium solar cell by spin-coating an organic transport layer onto the selenium photoabsorber attaining a power conversion efficiency of PCE=3.9%.[34]

Conclusion

In summary, we investigated the suitability of chemical bath deposited CdS as a heterojunction-partner for poly-Se and demonstrated the first functioning CdS/Se solar cell with an efficiency of PCE $\approx$ 1.14%. The energy band diagrams of the two semiconductors have been constructed using ultraviolet photoelectron spectroscopy combined with UV-Vis transmission measurements, showing a conduction band offset of 390 meV and a band bending of 380 meV. The difference in electron affinities combined with the proximity of the bandgap of CdS to that of poly-Se suggests that pure CdS is fundamentally a poor heterojunction partner for poly-Se, and while a chemical bath deposited buffer layer may enable an inversion of the device architecture, our findings indicate that an altogether different partner material

is needed to realize the full potential of poly-Se.

Acknowledgement

This work was supported by the Villum Foundation V-SUSTAIN grant (9455) to the Villum Center for the Science of Sustainable Fuels and Chemicals. The authors thank Prof. Brian Seger for fruitful discussions.

Supporting Information Available

Materials and characterization details, GIXRD patterns of a device at all processing steps, UV-Vis transmission measurements of various thicknesses of CdS, additional SEM top-view and cross-section images, JV and EQE measurements of all 6 devices in the batch, and full XPS and UPS surveys.

References

(1) Green, M. How Did Solar Cells Get So Cheap? *Joule* **2019**, *3*, 631–633.

(2) Bailie, C. D.; McGehee, M. D. High-efficiency tandem perovskite solar cells. *Mrs Bulletin* **2015**, *40*, 681–685.

(3) Kirchartz, T.; Rau, U. What Makes a Good Solar Cell? *Advanced Energy Materials* **2018**, *8*, 1703385.

(4) Green, M.; Dunlop, E.; Hohl-Ebinger, J.; Yoshita, M.; Kopidakis, N.; Hao, X. Solar cell efficiency tables (version 57). *Progress in Photovoltaics: Research and Applications* **2021**, *29*, 3–15.

(5) Shockley, W.; Queisser, H. Detailed Balance Limit Of Efficiency Of p-n Junction Solar Cells. *Journal of Applied Physics* **1961**, *32*, 510–519.

(6) Polman, A.; Knight, M.; Garnett, E. C.; Ehrler, B.; Sinke, W. C. Photovoltaic materials: Present efficiencies and future challenges. *Science* **2016**, *352*, aad4424.

(7) Green, M. A.; Bein, T. Perovskite cells charge forward. *Nature Materials* **2015**, *14*, 559–561.

(8) Wang, D.; Wright, M.; Elumalai, N. K.; Uddin, A. Stability of perovskite solar cells. *Solar Energy Materials and Solar Cells* **2016**, *147*, 255–275.

(9) K. Rao, M.; Sangeetha, D. N.; Selvakumar, M.; Sudhakar, Y. N.; Mahesha, M. G. Review on persistent challenges of perovskite solar cells' stability. *Solar Energy* **2021**, *218*, 469–491.

(10) Ward, J. S.; Remo, T.; Horowitz, K.; Woodhouse, M.; Sopori, B.; VanSant, K.; Basore, P. Techno-economic analysis of three different substrate removal and reuse strategies for III-V solar cells. *Progress in Photovoltaics: Research and Applications* **2016**, *24*, 1284–1292.

(11) Horowitz, K. A.; Remo, T. W.; Smith, B.; Ptak, A. J. *A Techno-Economic Analysis and Cost Reduction Roadmap for III-V Solar Cells*; Technical Report NREL/TP-6A20-72103, 2018.

(12) Youngman, T. H.; Nielsen, R.; Crovetto, A.; Seger, B.; Hansen, O.; Chorkendorff, I.; Vesborg, P. C. K. Semitransparent Selenium Solar Cells as a Top Cell for Tandem Photovoltaics. *Solar RRL* **2021**, 2100111.

(13) Bikowski, A.; Welzel, T.; Ellmer, K. The correlation between the radial distribution of high-energetic ions and the structural as well as electrical properties of magnetron sputtered ZnO:Al films. *Journal of Applied Physics* **2013**, *114*, 223716.

(14) Scheer, R.; Schock, H. W. *Chalcogenide Photovoltaics: Physics, Technologies, and Thin Film Devices*; Wiley-VCH, 2011; pp XV, 368.

(15) Wang, W.; Winkler, M. T.; Gunawan, O.; Gokmen, T.; Todorov, T. K.; Zhu, Y.; Mitzi, D. B. Device characteristics of CZTSSe thin-film solar cells with 12.6% efficiency. *Advanced Energy Materials* **2014**, *4*, 1301465.

(16) Romeo, A.; Artegiani, E. Cdte-based thin film solar cells: Past, present and future. *Energies* **2021**, *14*, 1684.

(17) Todorov, T. K.; Singh, S.; Bishop, D. M.; Gunawan, O.; Lee, Y. S.; Gershon, T. S.; Brew, K. W.; Antunez, P. D.; Haight, R. Ultrathin high band gap solar cells with improved efficiencies from the world's oldest photovoltaic material. *Nature Communications* **2017**, *8*, 682.

(18) Wanrooij, P. H.; Agarwal, U. S.; Meuldijk, J.; Van Kasteren, J. M.; Lemstra, P. J. Extraction of CdS pigment from waste polyethylene. *Journal of Applied Polymer Science* **2006**, *100*, 1024–1031.

(19) Zhu, M.; Niu, G.; Tang, J. Elemental Se: Fundamentals and its optoelectronic applications. *Journal of Materials Chemistry C* **2019**, *7*, 2199–2206.

(20) Hadar, I.; Song, T. B.; Ke, W.; Kanatzidis, M. G. Modern Processing and Insights on Selenium Solar Cells: The World's First Photovoltaic Device. *Advanced Energy Materials* **2019**, *9*, 1802766.

(21) Grätzel, M. Photoelectrochemical cells. *Nature* **2001**, *414*, 338–344.

(22) Anderson, R. L. Germanium-Gallium Arsenide Heterojunctions. *IBM Journal of Research and Development* **1960**, *4*, 283–287.

(23) Harrison, W. A.; Tersoff, J. Tight-Binding Theory Of Heterojunction Band Lineups Aand Interface Dipoles. *Journal of Vacuum Science and Technology B* **1986**, *4*, 1068–1073.

(24) Klein, A. Energy band alignment at interfaces of semiconducting oxides: A review of experimental determination using photoelectron spectroscopy and comparison with theoretical predictions by the electron affinity rule, charge neutrality levels, and the common anion rule. *Thin Solid Films* **2012**, *520*, 3721–3728.

(25) Minemoto, T.; Matsui, T.; Takakura, H.; Hamakawa, Y.; Negami, T.; Hashimoto, Y.; Uenoyama, T.; Kitagawa, M. Theoretical analysis of the effect of conduction band offset of window/CIS layers on performance of CIS solar cells using device simulation. *Solar Energy Materials and Solar Cells* **2001**, *67*, 83–88.

(26) Crovetto, A.; Cazzaniga, A.; Ettlinger, R. B.; Schou, J.; Hansen, O. Large process-dependent variations in band alignment and interface band gaps of Cu_2ZnSnS_4/CdS solar cells. *Solar Energy Materials and Solar Cells* **2018**, *187*, 233–240.

(27) Shaw, R. F.; Ghosh, A. K. SELENIUM HETEROSTRUCTURE SOLAR CELLS. *Solar Cells: Their Science, Technology, Applications and Economics* **1980**, *1*, 431–433.

(28) Ito, H.; Oka, M.; Ogino, T.; Takeda, A.; Mizushima, Y. Selenium Thin Film Solar Cell. *Japanese Journal of Applied Physics* **1982**, *21*, 77.

(29) Kephart, J. M.; Geisthardt, R. M.; Sampath, W. S. Optimization of CdTe thin-film solar cell efficiency using a sputtered, oxygenated CdS window layer. *Progress in Photovoltaics: Research and Applications* **2015**, *23*, 1484–1492.

(30) Ge, J.; Koirala, P.; Grice, C. R.; Roland, P. J.; Yu, Y.; Tan, X.; Ellingson, R. J.; Collins, R. W.; Yan, Y. Oxygenated CdS Buffer Layers Enabling High Open-Circuit Voltages in Earth-Abundant Cu2BaSnS4 Thin-Film Solar Cells. *Advanced Energy Materials* **2017**, *7*, 1601803 (10 pp.).

(31) Meysing, D. M.; Wolden, C. A.; Griffith, M. M.; Mahabaduge, H.; Pankow, J.; Reese, M. O.; Burst, J. M.; Rance, W. L.; Barnes, T. M. Properties of reactively

sputtered oxygenated cadmium sulfide (CdS:O) and their impact on CdTe solar cell performance. *Journal of Vacuum Science and Technology A: Vacuum, Surfaces and Films* **2015**, *33*, 021203.

(32) Duncan, D. A.; Kephart, J. M.; Horsley, K.; Blum, M.; Mezher, M.; Weinhardt, L.; Häming, M.; Wilks, R. G.; Hofmann, T.; Yang, W.; Bär, M.; Sampath, W. S.; Heske, C. Characterization of Sulfur Bonding in CdS:O Buffer Layers for CdTe-based Thin-Film Solar Cells. *Acs Applied Materials and Interfaces* **2015**, *7*, 16382–16386.

(33) Guo, L.; Zhang, B.; Li, S.; Montgomery, A.; Li, L.; Xing, G.; Zhang, Q.; Qian, X.; Yan, F. Interfacial engineering of oxygenated chemical bath–deposited CdS window layer for highly efficient Sb2Se3 thin-film solar cells. *Materials Today Physics* **2019**, *10*, 100125.

(34) Liu, W.; Said, A. A.; Fan, W. J.; Zhang, Q. Inverted Solar Cells with Thermally Evaporated Selenium as an Active Layer. *ACS Applied Energy Materials* **2020**, *3*, 7345–7352.

Graphical TOC Entry

Some journals require a graphical entry for the Table of Contents. This should be laid out "print ready" so that the sizing of the text is correct.
Inside the `tocentry` environment, the font used is Helvetica 8 pt, as required by *Journal of the American Chemical Society*.
The surrounding frame is 9 cm by 3.5 cm, which is the maximum permitted for *Journal of the American Chemical Society* graphical table of content entries. The box will not resize if the content is too big: instead it will overflow the edge of the box.
This box and the associated title will always be printed on a separate page at the end of the document.